Convolution Quadrature based BEM in acoustics for absorbing boundary conditions

Dominik Pölz[1], **Stefan Sauter**[2], and **Martin Schanz**[1]*

[1] Institute of Applied Mechanics, Graz University of Technology, Technikerstr. 4, 8010 Graz, Austria

[2] Institut für Mathematik, University of Zurich, Winterthurerstr. 190, CH-8057 Zürich, Switzerland

In many fields of engineering the acoustic behavior has to be determined, e.g. the sound distribution in a room or the sound radiation into the surrounding. Often, the goal is to obtain a sound pressure field such that disturbing noise is reduced to an acceptable level. In room acoustics, sound absorbing materials are often used to obtain this goal. The mathematical description is done with the wave equation and absorbing boundary conditions. The numerical treatment can be done with Boundary Element methods, where the absorbing boundary results in a Robin boundary condition. This boundary condition connects the Neumann trace with the Dirichlet trace of the time derivative.

Here, an indirect formulation, which uses the single layer potential, is used as basic boundary integral equation. The convolution quadrature method is applied for time discretisation, which allows a simple formulation of the Robin boundary condition in the Laplace domain. Convergence studies with a refinement in space and time show the expected rates. A realistic example for indoor acoustics, the computation of the sound pressure level in a staircase of the University of Zurich, show the suitability of this approach in determining the indoor acoustics. The absorbing boundary condition shows the expected behavior.

1 Governing equations

Let $\Omega^- \subset \mathbb{R}^3$ be a bounded Lipschitz domain with boundary $\Gamma := \partial\Omega$ and let $\Omega^+ := \mathbb{R}^3 \backslash \overline{\Omega^-}$ denote its unbounded complement. Let n denote the unit normal vector to Γ pointing into the exterior domain Ω^+. We consider the homogeneous wave equation (with constant sound speed c in the medium) for $\sigma \in \{+,-\}$

$$\begin{aligned} \partial_{tt} u - c^2 \Delta u &= 0 && \text{in } \Omega^\sigma \times \mathbb{R}_{>0}, \\ u(x,0) = \partial_t u(x,0) &= 0 && \text{in } \Omega^\sigma, \\ \gamma_1^\sigma(u) - \sigma \tfrac{\alpha}{c} \gamma_0^\sigma(\partial_t u) &= f(x,t) && \text{on } \Gamma \times \mathbb{R}_{>0}, \end{aligned} \tag{1}$$

where $\gamma_1^\sigma = \partial/\partial n$ is the normal derivative applied to a sufficiently smooth function in Ω^σ and γ_0^σ denotes the trace operator to Γ applied to a sufficiently smooth function in Ω^σ. If the domain $\Omega \in \{\Omega^-, \Omega^+\}$ is clear from the context we skip the superscript σ and simply write γ_1 and γ_0. In (1), α denotes the non-negative admittance, which is the inverse of the specific impedance of the surface Γ. This specific impedance is scaled by the density and the wave velocity. The mathematical analysis allows any non-negative finite value for α, however, realistic values are in the range $0 \leq \alpha \leq 1$. The lower limit modells a sound hard wall and the upper limit is a totally absorbing surface. Further, measured values show a frequency dependence and are listed in national design codes like the ÖNORM in Austria (ÖNORM EN 12354-6).

Such kind of absorbing boundary condition is the simplest possible choice to model the absorption of a surface. Certainly, more complicated models exist which take higher derivatives into account. The most realistic models consider an absorbing layer of porous material on the surface, which is computationally the most expensive model (see, e.g., [1,2]). Here, this simple model is used as it is common in real world applications.

We employ layer potentials to express the solution in terms of retarded potentials (cf. [3], [4], [5], [6]). The ansatz for the solution u as a single layer potential is given by

$$u(x,t) = (\mathcal{S} * \varphi)(x,t) := \int_\Gamma \frac{\varphi\left(y, t - \frac{\|x-y\|}{c}\right)}{4\pi \|x-y\|} d\Gamma_y \qquad \forall (x,t) \in \Omega^\sigma \times \mathbb{R}_{>0},$$

* Corresponding author: e-mail m.schanz@tugraz.at, phone +43 316 873 7600, fax +43 316 873 7641

which satisfies the first two equations in (1). The density φ then is determined via the third equation. The application of the trace γ_0 and normal trace γ_1 to u involves the following boundary integral operators

$$(\mathcal{V} * \varphi)(x,t) = \int_\Gamma \frac{\varphi\left(y, t - \frac{\|x-y\|}{c}\right)}{4\pi \|x-y\|} d\Gamma_y,$$
$$(\mathcal{K}' * \varphi)(x,t) = \frac{1}{4\pi} \int_\Gamma \frac{\langle n(x), y-x\rangle}{\|x-y\|^2} \left(\frac{\varphi\left(y, t - \frac{\|x-y\|}{c}\right)}{\|x-y\|} + \frac{\dot{\varphi}\left(y, t - \frac{\|x-y\|}{c}\right)}{c} \right) d\Gamma_y$$

for almost all $(x,t) \in \Gamma \times \mathbb{R}_{>0}$, more precisely, for all $(x,t) \in \Gamma \times \mathbb{R}_{>0}$, where Γ is smooth in a neighborhood of x. Then, it holds for $\sigma \in \{+,-\}$

$$\gamma_0^\sigma (\mathcal{S} * \varphi) = (\mathcal{V} * \varphi) \ , \qquad \gamma_1^\sigma (\mathcal{S} * \varphi) = -\left(\sigma \frac{\varphi}{2} - \mathcal{K}' * \varphi\right) \ ,$$

where, again, these equations hold almost everywhere on $\Gamma \times \mathbb{R}_{>0}$.

The third equation in (1) leads to the boundary integral equation for the single layer ansatz

$$-\left(\sigma \frac{\varphi}{2} - \mathcal{K}' * \varphi\right) - \sigma \frac{\alpha}{c} (\mathcal{V} * \dot{\varphi}) = f \quad \text{a.e. in } \Gamma \times \mathbb{R}_{>0}. \tag{2}$$

Certainly, also an integral equation using the double layer potential is possible.

The integral equation (2) is discretized in space and time. The spatial discretization follows the standard procedure. The geometrical discretization is done with linear triangles and the data are approximated by piecewise linear shape functions. The temporal discretization uses the convolution quadrature method (CQM) [7]. More precisely, the reformulated version of Banjai and Sauter [8] is applied, which works in principle as an inverse transformation [9]. This allows an easy realization of the time derivative in (2) as a simple multiplication by the Laplace variable.

All computations are done in 3-D and a normal BE formulation without any fast techniques is used. All regular integrals are performed with Gaussian quadrature formulas. The singular integrals are treated with the formulas of Erichsen and Sauter [10]. For the solution a direct solver is used. All implementations are done within the BE-library HyENA [11].

2 Numerical studies

The geometry chosen is a sphere with radius $1\,\mathrm{m}$ with a coordinate system fixed at the midpoint. The scattering into the outer air is considered and the respective analytical solutions can be determined using spherical harmonics as spatial function for the right hand side (see for the solution method [12]. Here, spherical harmonics of order $n = 0$, i.e. a constant, are chosen. The time behavior of the right-hand side is the bump function $f_m(t) = (ct)^m \mathrm{e}^{-ct}$. With this setting the density function is

$$\begin{aligned}\varphi^+(t) = -2(1+\alpha)^{m-1} \Bigg(& \left(\frac{2}{1+\alpha}\right)^m \mathrm{e}^{-2\left\{\frac{ct}{2}\right\}} \mathfrak{S}\left(\mathrm{e}^{-2}, \left\{\frac{ct}{2}\right\}, m, \left\lfloor \frac{ct}{2} \right\rfloor\right) \\ & - \frac{m!}{\alpha^{m+1}} \mathrm{e}^{-\frac{2}{1+\alpha}\left\{\frac{ct}{2}\right\}} \mathfrak{S}\left(\mathrm{e}^{-\frac{2}{1+\alpha}}, \left\{\frac{ct}{2}\right\}, 0, \left\lfloor \frac{ct}{2} \right\rfloor\right) \\ & + \frac{m!}{\alpha^{m+1}} \mathrm{e}^{-2\left\{\frac{ct}{2}\right\}} \sum_{k=0}^{m} \frac{1}{k!} \left(\frac{2\alpha}{1+\alpha}\right)^k \mathfrak{S}\left(\mathrm{e}^{-2}, \left\{\frac{ct}{2}\right\}, k, \left\lfloor \frac{ct}{2} \right\rfloor\right)\Bigg)\end{aligned}$$

using $\mathfrak{S}(a, \varepsilon, m, k)) := \sum_{\ell=0}^{k} (\ell+\varepsilon)^m a^\ell$ and the notation $\lfloor x \rfloor$ for the largest integer less than or equal to x and $\{x\} := x - \lfloor x \rfloor$ for the fractional part of x. The pressure solution is given for $ct > r - 1$

$$u^+(r,t) = \frac{m!}{2\sqrt{\pi} r} \frac{(1+\alpha)^m}{\alpha^{m+1}} \left(\mathrm{e}^{-(ct-r+1)} \sum_{k=0}^{m} \frac{\left(\frac{ct-r+1}{1+\alpha}\alpha\right)^k}{k!} - \mathrm{e}^{-\frac{ct-r+1}{1+\alpha}} \right) .$$

For all tests the material data from air at room temperature are used, i.e., $c = 343\,\mathrm{m/s}$ is set and the admittance is chosen to $\alpha = 0.5$. To characterise the relation between the spatial and temporal mesh the dimensionless parameter $\beta = c\Delta t/h$ is introduced where h denotes a characteristic element length (cathetus of the triangle) and Δt the constant time step size. The observation time is $(0, T = N\Delta t)$, where the final time is set to $T = 0.03\,\mathrm{s}$ in the following calculations.

The error compared to the analytical solution is measured only in time as the spatial behavior of the solution is constant due to the geometry and loading. In principle a discrete $L_2(0,T)$-error is realized by integrating numerically over time with

the Trapezoidal rule. This results in

$$\mathrm{err}_{abs} = \sqrt{\Delta t \sum_{n=0}^{N} \left(u\left(t_n\right) - u_h\left(t_n\right)\right)^2} \qquad \mathrm{err}_{rel} = \mathrm{err}_{abs} \left(\Delta t \sum_{n=0}^{N} \left(u\left(t_n\right)\right)^2\right)^{-\frac{1}{2}}, \tag{3}$$

evaluated at some arbitrary point on the surface for the density and at $x = (1.5, 0, 0)^T$ for the pressure field. The index $()_h$ indicates the numerical BE solution, whereas the other quantity is the respective exact solution. The order of the numerical convergence (eoc) is the relation $\mathrm{eoc} = \log_2\left(\frac{\mathrm{err}_h}{\mathrm{err}_{h+1}}\right)$, where the indices $()_h$ and $()_{h+1}$ denotes two subsequent refinement levels. For the following tests three different meshes of the sphere are used with element length of $h_1 = 0.224\,\mathrm{m}, h_2 = 0.112\,\mathrm{m}$, and $h_3 = 0.056\,\mathrm{m}$. The triangles are uniformly refined by subdividing.

In Fig. 1, the $L_2(0,T)$-error for the density is plotted versus the mesh size for different multistep methods (BDF 1 and BDF 2) and different values of β. The eoc is given with a dashed-dotted line to have a comparison. The results show that the method converges with a rate of ≈ 1.2 for BDF 2 and a smaller rate of ≈ 0.75 for BDF 1. The $L_2(0,T)$-error for the pressure solution at the inner point $x = (1.5, 0, 0)^T$ is given in Fig. 2. As expected the error in the domain has a better behavior and the rate of convergence is higher, i.e. ≈ 2 for BDF 2 and ≈ 1.4 for BDF 1.

As an realistic example the influence of absorbing layers in room acoustics is studied. In 2010/11, the atrium of the "Institut für Mathematik" at the University Zürich (see Fig 3) has been acoustically successfully improved by installing

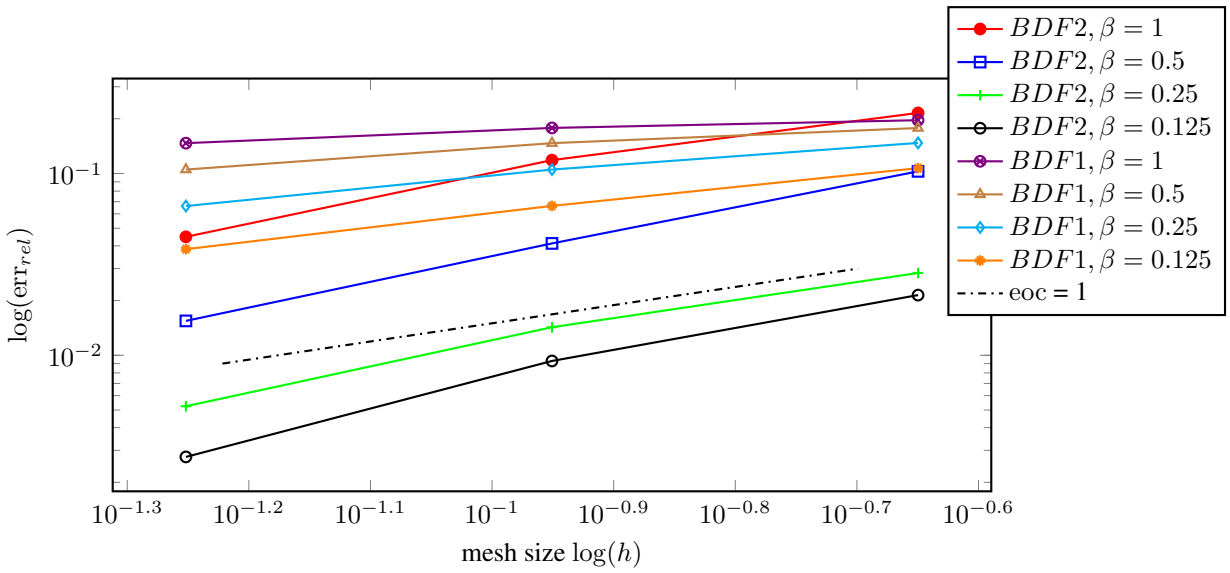

Fig. 1: Relative error of the density for different meshes

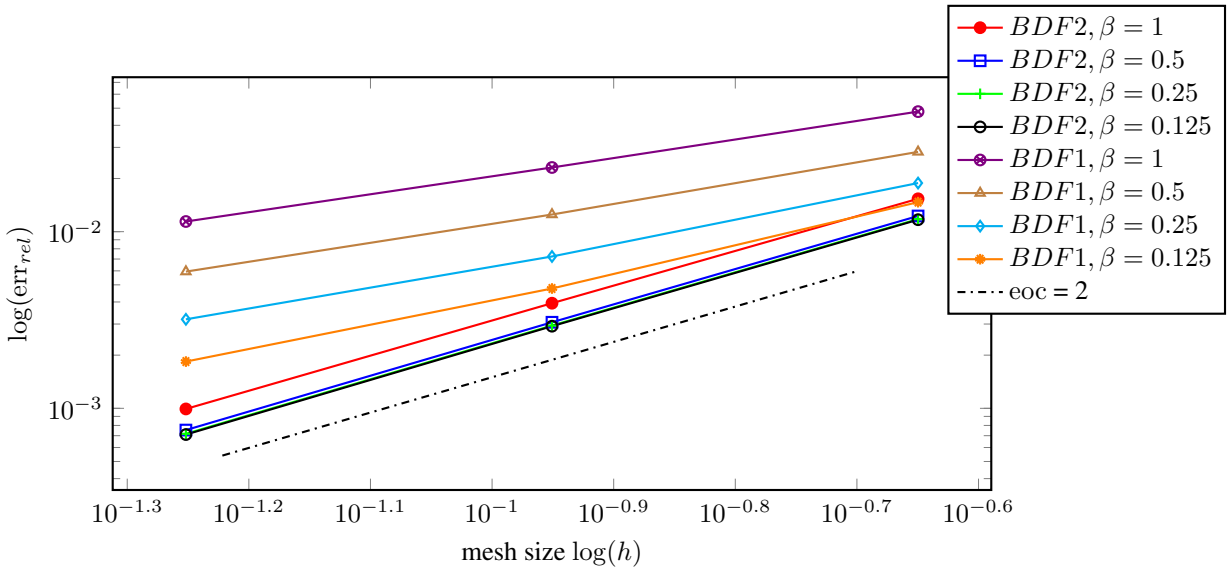

Fig. 2: Relative error of the pressure solution

Fig. 3: The atrium of the "Institut für Mathematik" at the University Zürich

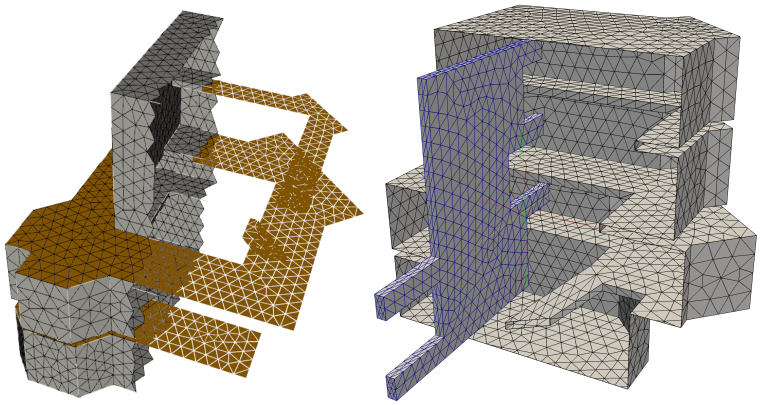

Fig. 4: Mesh for the atrium cut in two halfs to show the interior and the location of the absorbers (brown area)

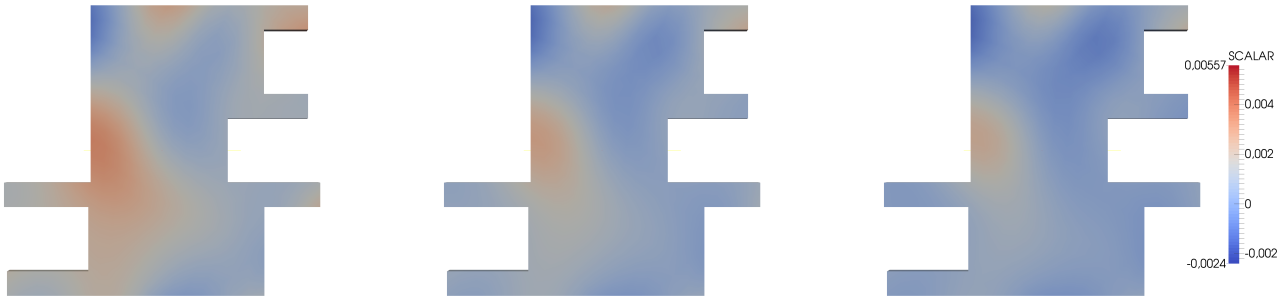

(a) $\alpha = 0.05$ **(b)** $\alpha = 0.40$ **(c)** $\alpha = 0.80$

Fig. 5: Pressure distribution at time $t = 0.096\,\mathrm{s}$ in the interior of the atrium for different absorption coefficients

absorber panels at the ceilings in the floors (see the brown areas in the mesh of Fig. 4). This action was successful and the following computation tries to model this positive effect. The mesh shown in Fig. 4 is used and, here, a double layer ansatz has been applied. The excitation is an incoming wave from the top area of the atrium. The effect of the absorbing layers can be seen in Fig. 5, where the sound pressure in the interior of the atrium is depicted for different values of the admittance α. It can clearly be observed that materials with higher absorption reduce the sound pressure level significantly.

References

[1] A. Franck and M. Aretz, Wall structure modeling for room acoustic and building acoustic fem simulations, in: Proc. of 19th International Congress on Acoustics, (2007).
[2] L. Nagler, P. Rong, M. Schanz, and O. v. Estorff, Comput. Mech. **53**(4), 549–560 (2014).
[3] J. Stratton, Electromagnetic Theory (McGraw-Hill, New York, 1941).
[4] M. Friedman and R. Shaw, J. Appl. Mech. **29**, 40–46 (1962).
[5] A. Bamberger and T. Ha-Duong, Math. Meth. Appl. Sci. **8**, 405–435 and 598–608 (1986).
[6] F. J. Sayas, Retarded Potentials and Time Domain Boundary Integral Equations: A Road Map (Springer Verlag, 2016).
[7] C. Lubich, Numer. Math. **52**, 129–145 (1988).
[8] L. Banjai and S. Sauter, SIAM J. Numer. Anal. **47**(1), 227–249 (2008).
[9] M. Schanz, CMES Comput. Model. Eng. Sci. **58**(2), 109–128 (2010).
[10] S. Erichsen and S. A. Sauter, Comput. Methods Appl. Mech. Engrg. **157**(3–4), 215–224 (1998).
[11] M. Messner, M. Messner, F. Rammerstorfer, and P. Urthaler, Hyperbolic and elliptic numerical analysis BEM library (HyENA), `http://www.mech.tugraz.at/HyENA`, 2010, [Online; accessed 22-January-2010].
[12] S. Sauter and A. Veit, IMA J. Numer. Anal. **34**(2), 675–699 (2013).